ELSEVIER

Chemical Engineering Journal 138 (2008) 578–585

Chemical Engineering Journal

www.elsevier.com/locate/cej

Modification of magnetite nanoparticles via surface-initiated atom transfer radical polymerization (ATRP)

Yang Zhou [a,b,*], Shixing Wang [a,b], Bingjun Ding [a], Zhimao Yang [a]

[a] *Department of Materials Physics, School of Science, Xi'an Jiaotong University, Xi'an 710049, China*
[b] *National Centre for Nanoscience and Technology, Beijing 100080, China*

Received 7 April 2007; received in revised form 28 June 2007; accepted 5 July 2007

Abstract

Modification of magnetite nanoparticles via surface-initiated atom transfer radical polymerization (ATRP) was carried out. The magnetic nanoparticles with an initiator group for copper-mediated atom transfer radical polymerization, 3-aminopropyltriethoxysilane chemically bound on their surfaces were prepared by the self-assembled monolayer. Well defined diblock copolymer brushes consisting of poly(ethylene glycol) methacrylate and methyl methacrylate blocks were obtained by using the initial homopolymer brushes as the macroinitiators for the ATRP of the second monomer. The chemical composition of the functionalized magnetite nanoparitcles was characterized by X-ray photoelectron spectroscopy, FT-IR spectroscopy and thermogravimetric analysis. The difference of proteins non-specifically adsorbed onto the surface of uncoated and functionalized magnetite nanoparticles was evaluated. The ability of the functionalized magnetite nanoparticles to resist the proteins non-specific adsorption was higher than that of uncoated nanoparticles.

Keywords: Magnetite nanoparticle; Surface modification; Silanization reaction; Atom transfer radical polymerization; Graft polymerization

1. Introduction

Magnetite nanoparticles (Fe_3O_4, MNPs) are widely studied due to their potential applications in biology and medicine such as enzyme and protein immobilization, magnetic cell separation and purification, magnetic resonance imagine (MRI), RNA and DNA purification and magnetically controlled transport of anticancer drugs [1–6]. For many applications, the control of surface functionality is a key for controlling the nanoparticle's interaction with biological species, self-assembly dispersion and compatibility with polymeric materials. MNPs may undergo rapid biodegradation when they are directly exposed to the biological system [7,8]. Therefore, to prevent such limitations and in order to be used for biomedical purposes, magnetite must be precoated with substances that make them stable, biocompatible, non-toxic in physiological medium and able to be bound to complex biological molecules, such as monoclonal antibodies, lectings, peptides, hormones, vitamins, nucleotides, or drugs [9].

Several methods have been developed to prepare polymer-coatings on magnetite nanoparticles such as physical adsorption of polymers, emulsion polymerization in the presence of nanoparticles, and the so-called "grafting to" and "grafting from" methods [10–13]. Silane chemistry has been applied to metal oxide surfaces to promote metal–metal and metal–polymer adhesion. Previous literatures [14–16] have demonstrated the formation of polysiloxanes on the surface of magnetite via alkylalkoxylianes self-assembly. Atom transfer radical polymerization (ATRP) is a recently developed "living" or "controlled" radical polymerization method [17–19], which does not require stringent experimental conditions. ATRP allows for the polymerization and block copolymerization of a wide range of functional monomers such as styrenes, (meth)acrylates, (meth)acrylamides, and (meth)acrylic acids [20] in a controlled fashion, yielding polymers with narrowly dispersed molecular weights. Moreover, ATRP is tolerant of monomers with polar functionality. Thus, it allows the direct polymerization of functional monomers without involving the tedious protection and deprotection procedures.

In this work, we have applied copper-mediated ATRP technique to graft polymerization of poly(ethylene glycol) methacrylate (PEGMA) and poly(ethylene glycol)methacrylate-

* Corresponding author at: Department of Materials Physics, School of Science, Xi'an Jiaotong University, Xi'an 710049, China. Tel.: +86 29 8266 5995; fax: +86 29 8266 0901.
E-mail address: zhouyang8250@sohu.com (Y. Zhou).

1385-8947/$ – see front matter © 2007 Elsevier B.V. All rights reserved.
doi:10.1016/j.cej.2007.07.030

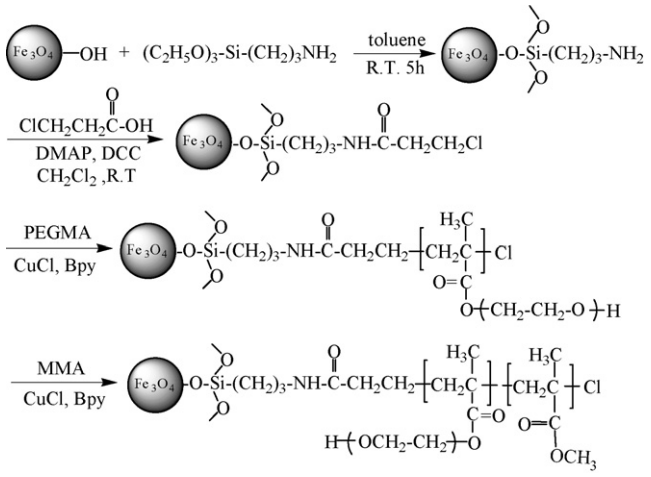

Fig. 1. Schematic diagram illustrating the processes of silanization of the Fe_3O_4 surface to give rise to the Fe_3O_4-Cl surface, surface-initiated ATRP of PEGMA-b-MMA block copolymer brushes from the Fe_3O_4-Cl surface.

b-methyl methacrylate (PEGMA-b-MMA) block copolymers on MNPs with an ATRP initiator immobilized on their surface. The biocompatibility of MNPs could be greatly improved by introducing a monolayer of low molecular weight poly(ethylene glycol) (PEG) to their surface [21]. PEGylated MNPs have proven to be non-immunogenic, non-antigentic and protein resistant [22,23]. In addition, the end hydroxyl groups of the grafted PEGMA polymer (P(PEGMA)) side chains can be converted into various functional derivatives [24]. For this reason, we chose PEGMA as monomer to be polymerized on the surface of MNPs. In order to confirm that ATRP is "living" or "controlled" radical polymerization method, we also chose MMA as monomer to be continued polymerized on the surface of MNPs with surface grafted P(PEGMA). This work has potential for the development of smart materials based on MNPs bearing surface grafted versatile properties polymer. The processes of immobilization of the ATRP initiator via the silane coupling agent and the subsequent surface-initiated ATRP are shown schematically in Fig. 1.

2. Experimental

2.1. Materials

3-Aminopropyltriethoxysilane (APTES), poly(ethylene glycol) monomethacrylate macromonomer (PEGMA, $n = 6$, $M_n \sim 360$ g/mol, >99%), methyl methacrylate (MMA) (99%), 2,2′-byridine (Bpy, 99%), 1,3-dicyclohexylcarbodiimide (DCC), 4-dimethylaminopyridine (DMAP) were purchased from Aldrich Chemical Co. PEGMA, MMA monomers were distilled under reduced pressure over CaH_2 prior to use. Ferric chloride hexahydrate ($FeCl_3 \cdot 6H_2O$, >98%) and ferrous chloride tetrahydrate ($FeCl_2 \cdot 4H_2O$ >99%), toluene, *N*,*N*-dimethylformamide (DMF), copper(I) chloride (99%), dichloromethane (DCM), and 3-chloropropionic acid were obtained from China National Medicines Corporation Ltd. and used as received.

2.2. Preparation of the magnetic nanoparticles

MNPs were prepared without any additional stabilizer according to the following procedure. Briefly, a solution (50 mL) of mixture of $FeCl_2$ (0.1 M) and $FeCl_3$ (0.2 M) (molar ratio 1:2) was added dropwise into 250 mL of alkali solution (0.1 M NaOH) under vigorous mechanical stirring for 30 min at room temperature. The color of the suspension turned black immediately. The precipitated powders were collected by magnetic separation. Distilled water was added to wash the powder four times followed by the addition of a 0.01 M HCl solution to neutralize the anionic charge on the surface of particles. The positively charged colloidal particles were obtained by magnetic separation. Then MNPs were dried into powder at 40 °C under vacuum.

2.3. Immobilization of the initiator on the Fe_3O_4 surface

The surface of Fe_3O_4 was coated with 3-aminopropyltriethoxysilane by a silanization reaction to obtain modified MNPs according to previous report [14]. Namely, 3.7 g of MNPs were mixed with toluene (40 mL) using ultrasonic to produce a homogeneous suspension, to which 19.5 mmol of APTES were added using a syringe. The reaction mixture was kept at room temperature for 5 h under nitrogen atmosphere with vigorous mechanical stirring. Then obtained APTES-immobilized MNPs were washed with ethanol (2× 30 mL) and DCM (2× 30 mL) in turn. After magnetic separation, the silanized MNPs were used to immobilize the initiator. Briefly, 15.9 mmol APTES-modified MNPs (Fe_3O_4-APTES) were suspended in 100 mL of DCM, to which 31.8 mmol of 3-chloropropionic acid, DCC (6.61 g, 31.8 mmol) and DMAP (0.39 g, 3.18 mmol) were added, respectively. The reaction mixture was refluxed for 4 h at 60 °C under nitrogen atmosphere with vigorous mechanical stirring. After reaction, the mixture was cool down to room temperature and magnetic separated. The chloro-functionalized MNPs (Fe_3O_4-Cl) were washed with methanol (2× 40 mL) and distilled water (2× 40 mL), respectively. They were then dried in a clean vacuum oven at 40 °C overnight.

2.4. Surface-initiated atom transfer radical polymerization

For the preparation of PEGMA polymer brushes on the Fe_3O_4-Cl surface, the following procedures were carried out. Two grams of Fe_3O_4-Cl were dispersed in 80 mL of DMF, to which PEGMA (10 mL, 30 mmol), CuCl (30 mg, 0.3 mmol) and Bpy ligand (90 mg, 0.6 mmol) were added. The reaction was carried out at 70 °C water bath for 4 h under nitrogen atmosphere with vigorous mechanical stirring. After the reaction, the MNPs with surface grafted P(PEGMA) (Fe_3O_4-g-P(PEGMA)) were magnetic separated and washed thoroughly with an excess amount of distilled water.

For the preparation of P(PEGMA)-b-P(MMA) block copolymer brushes on the MNPs surface, the Fe_3O_4-g-P(PEGMA) was used instead of Fe_3O_4-Cl under the same polymerization con-

ditions as those described above for the surface-initiated ATRP of PEGMA.

2.5. Surface characterization

X-ray diffraction (XRD) measurements were carried out with a RIGAKU D/MAX-2400 with Cu Kα (40 kV) radiation. Electron micrographs of the samples were obtained by a JEM-3010 high-resolution transmission electron microscope.

X-ray photoelectron spectroscopy was performed on an ESCALab220i-XL electron spectrometer from VG Scientific using 300 W Al Kα radiation. The base pressure was about 3×10^{-9} mbar. The binding energies were referenced to the C 1s line at 284.8 eV from adventitious carbon. In curve fitting, the line width (full width at half-maximum, or fwhm) for the Gaussian peaks was maintained constant for all components in a particular spectrum.

Fourier transform infrared (FT-IR) spectra were obtained using Spectrum One FT-IR spectrometer (Perkin Elmer) with a resolution of 4 cm^{-1}. To characterize the layers formed on the surface on MNPs, a small amount of nanoparticle powder was milled with KBr, and the mixture was pressed into a disk for analysis. Protein plasma absorption data were measured at room temperature with a Varian Cary 100 UV–vis spectrophotometer using 1 cm path length and 100 μL capacity black-body quartz cuvettes.

Thermogravimetric analysis (TGA) was carried out using Pyris TG/DTA (Perkin Elmer) thermogravimetric analyzer at a heating rate of 10 °C/min under a flow of nitrogen.

Magnetization measurements were obtained at room temperature using a vibrating sample magnetometer (VSM, Lakeshore 7307) with a maximum magnetic field of 10 kOe.

2.6. Protein resistance test

Lysozyme (from chicken egg, MW 14.3 kDa), γ-globulins (from bovine, MW 150 kDa), fibrinogen (from human, MW 340 kDa) and bovine serum albumin (BSA, from bovine, MW 66 kDa) were purchased from Sigma-Aldrich Co. and used as model proteins for the protein adsorption assay. These proteins represent a wide range of proteins found in body fluids with different physical properties. In addition, the basic information on these proteins including their isoelectric points, molecular weights, and their general solution behavior is well established [25]. Protein solutions were obtained by dissolving the protein in phosphate buffered saline (PBS, pH 7.4) at a concentration of 2.5 mg/mL. The concentration of uncoated Fe_3O_4 and Fe_3O_4-g-P(PEGMA)-b-P(MMA) suspension was 4 mg/mL by dispersed 40 mg of magnetite nanoparticles in 10 mL of PBS respectively with ultrasonic vibration for 30 min. Then 20 μL of protein solution was added to a 1.5 mL Eppendorf tube with 100 μL of magnetite suspension in 80 μL of PBS. At 4 °C, the mixture was incubated for 5 h. The UV–vis spectrophotometer was used to determine the amount of adsorbed proteins.

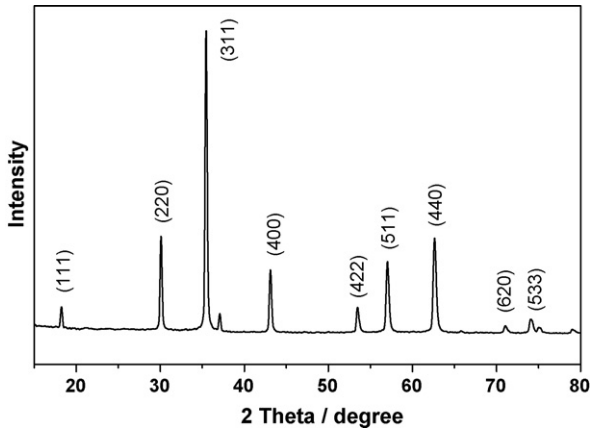

Fig. 2. X-ray powder diffraction patterns of Fe_3O_4 nanoparticles.

3. Results and discussion

3.1. Characterization of Fe_3O_4 nanoparticles

Fig. 2 shows a XRD pattern of Fe_3O_4 nanoparticles which indicates a highly crystalline cubic spinel structure. The reflection peak positions and relative intensities of Fe_3O_4 nanoparticles agree well with the XRD patterns of MNPs in the literatures [26,27], which confirm the structure of the magnetite materials. The average size of the Fe_3O_4 nanoparticles deduced from Sherrer's formula based on Fig. 2 is about 22 nm, which is consistent with the result obtained from the transmission electron microscopy (Fig. 3a) analysis of the same sample. The electron diffraction pattern (inset in Fig. 3a) consisting of rings indicates the good crystal structure of the nanoparticles. The TEM image of P(PEGMA)-b-P(MMA) coated MNPs is shown in Fig. 3b, which indicates the average size of nanoparticles is 20 ± 0.8 nm. Table 1 shows the measured lattice spacing based on the rings in the electron diffraction pattern, and the results accord with the known lattice spacing for bulk Fe_3O_4

Table 1
Measured lattice spacing, *d* (nm), based on the ED (inset in Fig. 2)

	1	2	3	4	5	6	7	8	9
d	0.485	0.296	0.253	0.209	0.171	0.161	0.148	0.132	0.127
Fe_3O_4	0.486	0.297	0.253	0.210	0.171	0.162	0.148	0.133	0.128
h k l	111	220	311	400	422	511	440	620	533

Standard atomic spacing for Fe_3O_4 along with their respective *h k l* indexes from the PDF database [28].

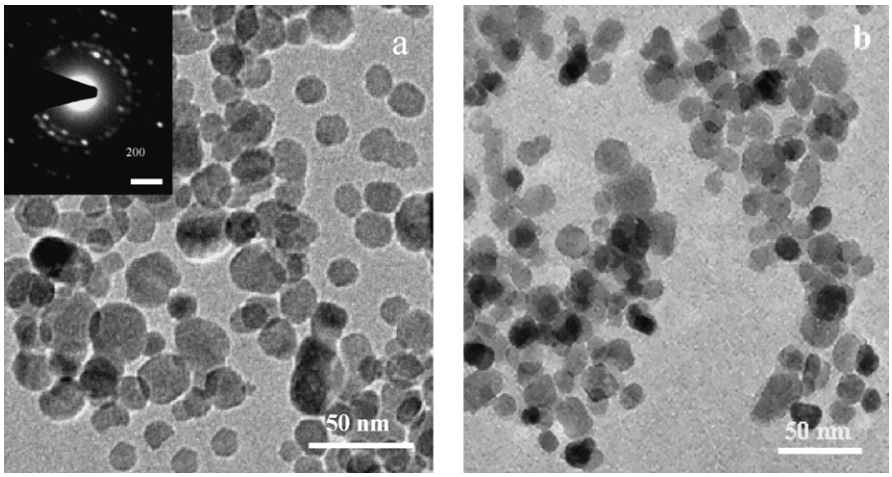

Fig. 3. TEM images of (a) Fe_3O_4 nanoparticles (inset is electron diffraction pattern) and (b) Fe_3O_4-g-P(PEGMA)-b-P(MMA).

along with their respective *h k l* indexes from the PDF database [28].

3.2. Immobilization of the ATRP initiator on the Fe_3O_4 nanoparticles via a silane coupling reagent

To obtain the immobilization of the ATRP initiator on the MNPs, APTES was immobilized on the surface of Fe_3O_4 via ligand-exchanging reaction between the hydroxyl groups on the MNPs and triethoxyliane groups of APTES to form a bond between the magnetite and the silane compound [29]. Then, the Fe_3O_4-APTES was used as precursor to immobilize the ATRP initiator to form Fe_3O_4-Cl. The introduction of initiator onto MNPs was confirmed by XPS analysis.

Fig. 4a and b show the wide-scan spectra of the Fe_3O_4 nanoparticles and functionalized Fe_3O_4-Cl surfaces, respectively. The wide-scan spectrum of the Fe_3O_4 surface is dominated by signals attributable to Fe, O, and C. Fig. 4c and d show Si 2p and N 1s core-level spectra of Fe_3O_4-APTES. Silane coupling agent immobilized on Fe_3O_4 can make a condensation reaction with 3-chloropropionic acid to produce a stable initiator monolayer, consistent with the appearance of the Si, N and Cl signals in the wide-scan spectrum of Fe_3O_4-Cl surface in

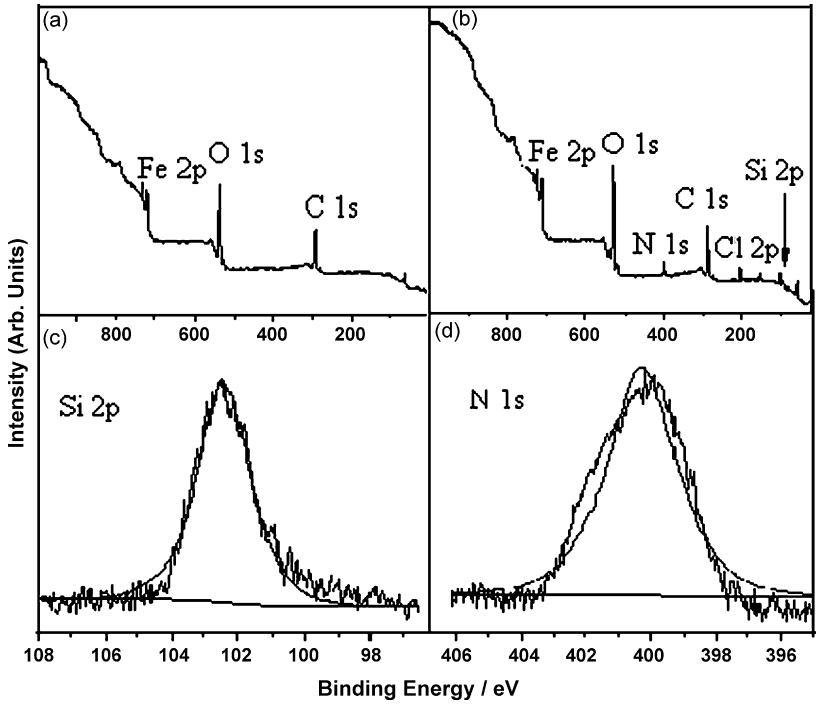

Fig. 4. Wide-scan spectra of the Fe_3O_4 nanoparticles surface (a), Fe_3O_4-Cl nanoparticles surface (b) and Si 2p (c), N 1s (d) core-level spectra of the functionalized Fe_3O_4-Cl surfaces.

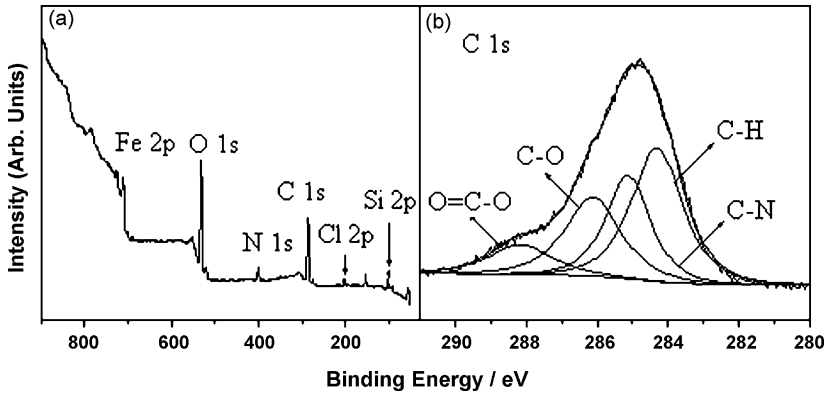

Fig. 5. Wide-scan (a) and C 1s core-level (b) spectra of Fe_3O_4-g-P(PEGMA) surface.

Fig. 4b. The XPS results confirm the success of the formation of Fe_3O_4-Cl nanoparticles, that is, the immobilization of the surface-initiator.

3.3. Surface-initiated ATRP of PEGMA on magnetite nanoparticles

The Fe_3O_4 surface with grafted P(PEGMA) brushes is referred to as the Fe_3O_4-g-P(PEGMA). Fig. 5a and b show the respective wide-scan and C 1s core-level spectra of the Fe_3O_4-g-P(PEGMA) surface after polymerization time of 4 h. The persistence of the Cl species in wide-scan spectrum is consistent with the fact that polymerization via ATRP involves a "living" chain end, consisting of a dormant alkyl halide species, that can be used to initiate the subsequent block copolymerization. The appearance of C–O and O=C–O components confirms that P(PEGMA) has been successfully grafted on the Fe_3O_4-Cl surface.

3.4. Surface-initiated ATRP of PEGMA-b-MMA copolymer on magnetite nanoparticles

One of the unique characteristics of the polymers synthesized by ATRP is the preservation of the active or "living" end groups throughout the polymerization reaction. To further confirm the presence of active chain ends in the grafted PEGMA polymer, diblock copolymer brushes consisting of P(PEGMA) and P(MMA) blocks were prepared by using the P(PEGMA) brushes already on the Fe_3O_4-Cl surface (Fig. 1) as the macroinitiator for the ATRP of the second monomer, MMA. The formation of block copolymer brushes was confirmed by XPS.

The wide-scan and C 1s core-level spectra of the Fe_3O_4-g-P(PEGMA)-b-P(MMA) surface (4 h of surface-initiated ATRP of PEGMA from the Fe_3O_4-Cl surface and then 4 h of surface-initiated ATRP of MMA from the as-prepared Fe_3O_4-g-P(PEGMA) surface) are shown in Fig. 6a and b, respectively. The C 1s core-level spectrum can be curve-fitted with four peak components having binding energies at about 284.6, 285.5, 286.2, and 288.5 eV attributable to the C–H, C–N, C–O, and O=C–O species, respectively. Comparison of C 1s core-level spectrum of Fig. 6b to that of the Fe_3O_4-g-P(PEGMA) surface in Fig. 5b reveals that the intensity of the C–O and O=C–O peak components have increased significantly after the block copolymerization of MMA. Moreover, the C 1s core-level line shape in Fig. 6b is similar to that of the Fe_3O_4-g-P(PEGMA) surface of Fig. 5b, suggesting that the Fe_3O_4-g-P(PEGMA)-b-P(MMA) surface is dominated by the P(PEGMA) blocks.

Fig. 7 shows the TGA thermograms for uncoated and modified MNPs. The magnetic nanoparticles after each stage of modification give their distinctive TGA curves, which provide approximate amount of P(PEGMA) and P(MMA) on the MNPs. The absolute weight loss of the uncoated MNPs is 2.2% for the whole temperature range because of the removal of adsorbed physical and chemical water. Fig. 7b shows the weight loss

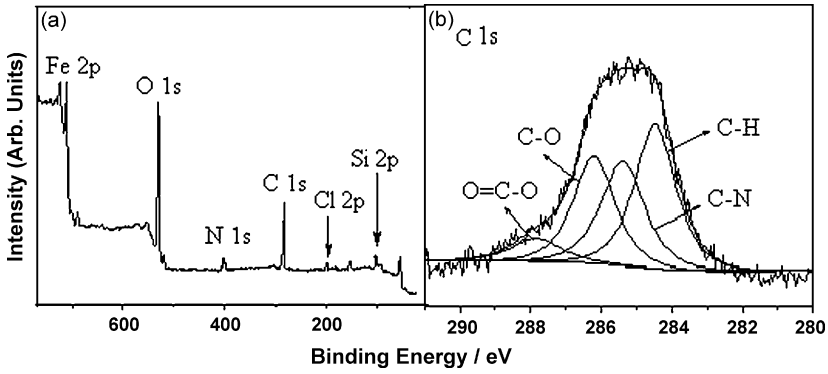

Fig. 6. Wide-scan and C 1s core-level spectra of Fe_3O_4-g-P(PEGMA)-b-P(MMA) surface.

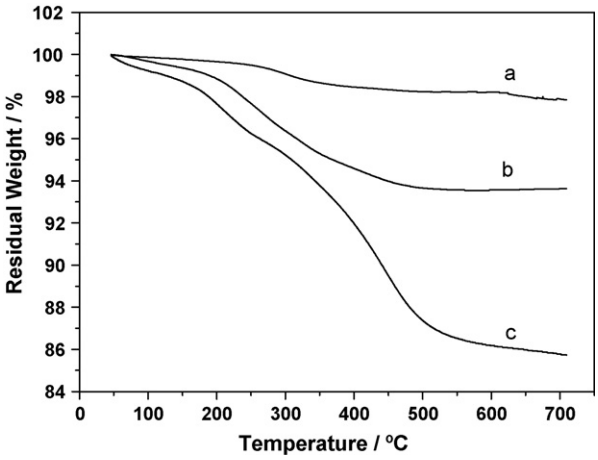

Fig. 7. TGA curves of (a) uncoated Fe_3O_4, (b) Fe_3O_4-APTES and (c) Fe_3O_4-g-P(PEGMA)-b-P(MMA).

increased above 230 °C, attributed to the loss of the APTES layer. It is estimated that the weight loss of APTES coated on the MNPs is about 6.5%. As shown in Fig. 7c, the first stage shows a weight loss of about 4.6% at 270 °C while the second stage accounts for 9.7% of the another weight loss. These two stages weight loss indicates the degradation of P(MMA) and P(PEGMA) on the surface of MNPs, respectively.

The saturation magnetization value of the uncoated MNPs is 67.9 emu/g at 25 °C, and neither remanence nor coercivity is observed (Fig. 8a), which indicates that the as-synthesized MNPs are superparamagnetic. Superparamagnetism (i.e. the nanoparticles would not retain any magnetism after removed of the magnetic field) is an especially important property needed for magnetic targeting carriers. As shown in Fig. 8b, no remanence or coercivity is also observed with Fe_3O_4-g-P(PEGMA)-b-P(MMA). The saturation magnetization value is 61.3 emu/g. This large saturation magnetization of MNPs makes them very susceptible to magnetic fields and therefore makes the solid and liquid phase separate easily.

The surface modification of MNPs with P(PEGMA)-b-P(MMA) was confirmed by FT-IR, as shown in Fig. 9 together

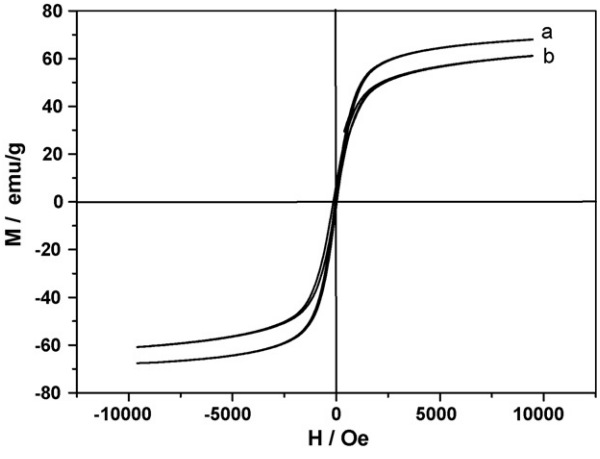

Fig. 8. Room temperature magnetization curves of as-synthesized and functionalized MNPs: (a) uncoated Fe_3O_4 and (b) Fe_3O_4-g-P(PEGMA)-b-P(MMA).

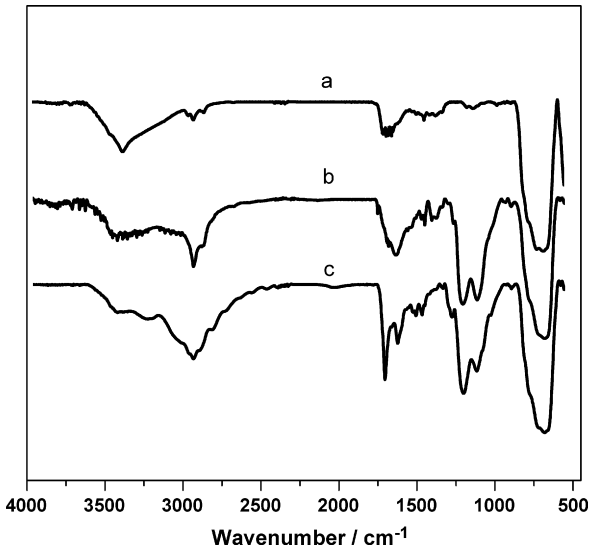

Fig. 9. FT-IR spectra of (a) uncoated Fe_3O_4, (b) Fe_3O_4-APTES and (c) Fe_3O_4-g-P(PEGMA)-b-P(MMA).

with the FT-IR spectra of uncoated and silane-coated nanoparticles. The introduction of APTES to the surface of MNPs was confirmed by the bands at 1113 and 1036 cm^{-1} assigned to the Si–O groups. The two broad bands at 3417 and 1625 cm^{-1} can be ascribed to the N–H stretching vibration and NH_2 bending mode of free NH_2 groups, respectively. The presence of the anchored propyl group was confirmed by C–H stretching vibration that appeared at 2930 and 2862 cm^{-1}. The FT-IR spectrum of Fe_3O_4-g-P(PEGMA)-b-P(MMA) showed a broad band at 1130 cm^{-1} attributed to the C–O–C ether stretch band. The spectrum also showed a strong band around 2912 cm^{-1} corresponding to the CH_2 stretching vibrations. The ester group was cleared observed at 1735 cm^{-1}. No strong absorption band at around 1630 cm^{-1}, which is the characteristic band for C=C stretching vibration of the PEGMA and MMA monomer, can be found from Fig. 9c. The absence of C=C stretching vibration further confirmed the graft polymerization of the PEGMA and MMA monomer on the magnetic nanoparticles.

3.5. Non-specific adsorption test

To evaluate the resistance of the uncoated Fe_3O_4 and Fe_3O_4-g-P(PEGMA)-b-P(MMA) against the adsorption of various proteins, we investigated the adsorption of four proteins, fibrinogen, BSA, γ-globulins and lysozyme, which have different molecular weights. We measured the optical absorption of supernatant liquid for uncoated Fe_3O_4 and Fe_3O_4-g-P(PEGMA)-b-P(MMA) after incubation for 5 h in different protein solutions by UV–vis spectroscopy. The UV–vis absorbance of proteins was different from the results of the control experiments, which indicated that the concentration of proteins decreased because of the adsorption onto the surface of Fe_3O_4. As given in Fig. 10, the absorbance intensity of the Fe_3O_4-g-P(PEGMA)-b-P(MMA) solution incubated with proteins are 80, 91.1, 90.7, and 79.5% of BSA, fibrinogen, lysozyme and γ-globulins, respectively, which were higher

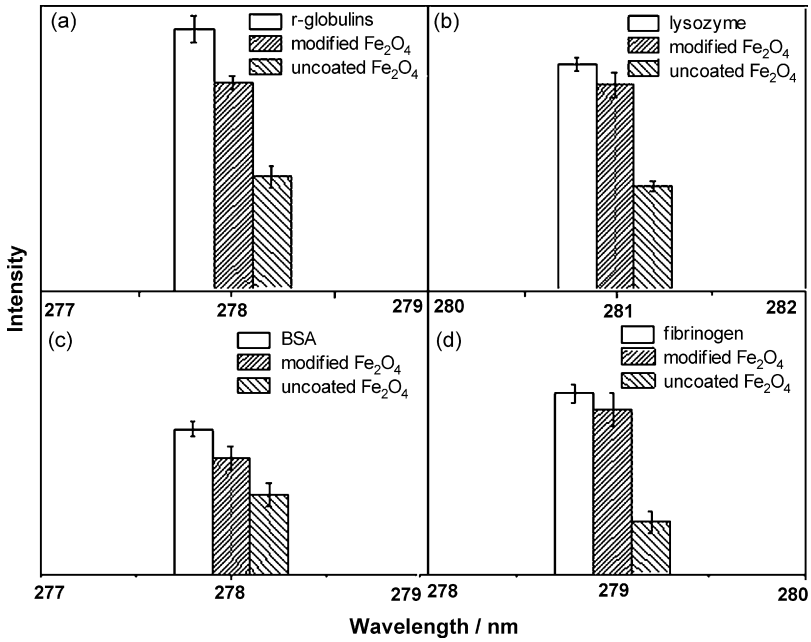

Fig. 10. The non-specific adsorption of different proteins on the surface of uncoated Fe_3O_4 and Fe_3O_4-g-P(PEGMA)-b-P(MMA): (a) γ-globulins, (b) lysozyme, (c) BSA and (d) fibrinogen. The concentration of proteins is 0.25 mg/mL and the mixture incubates at 4 °C for 5 h.

than that of uncoated Fe_3O_4. Taking the valuation results together, Fe_3O_4 coated with P(PEGMA)-b-P(MMA) was shown to reduce the proteins non-specific adsorption to the surface of Fe_3O_4. In particular, the ability of Fe_3O_4-g-P(PEGMA)-b-P(MMA) nanoparticles to resist the adsorption of fibrinogen was higher than that of uncoated Fe_3O_4, showing 62.3 percentage points increase in absorbance intensity. So these P(PEGMA)-b-P(MMA) coated MNPs have the potential application to prolong the circulation time by minimizing or eliminating the protein adsorption to the nanoparticles in drug delivery and releases.

4. Conclusions

Immobilization of an ATRP initiator on the Fe_3O_4 surface via the action of 3-aminopropyltriethoxysilane coupling reagent allowed the subsequent surface-initiated ATRP to produce functional polymer brushes. The "dormant" chain ends of the polymer brushes on the Fe_3O_4 surface could be used as macroinitiators for further functionalization of the hybrid surfaces via block copolymerization to produce alternate polymer layers of different properties. Fe_3O_4-g-P(PEGMA)-b-P(MMA) shows higher ability for resistance of proteins than that of uncoated Fe_3O_4. The Fe_3O_4-polymer hybrids prepared via surface-initiated ATRP thus combine the advantages of Fe_3O_4 with the advantages of the grafted polymer/copolymer chains, which are potential useful to the fabrication of Fe_3O_4-based medical and biomedical devices.

Acknowledgement

Financial support of this work from the National Nature Science Foundation of China (No. 50471033 and 50537070) is gratefully acknowledged.

References

[1] A.K. Gupta, M. Gupta, Biomaterials 26 (2005) 3995–4021.
[2] C.J. Xu, K.M. Xu, H.W. Gu, R.K. Zheng, H. Liu, X.X. Zhang, Z.H. Guo, B. Xu, J. Am. Chem. Soc. 126 (2004) 9938–9939.
[3] H.W. Gu, K.M. Xu, C.J. Xu, B. Xu, Chem. Commun. (2006) 941–949.
[4] Z.M. Saiyed, C. Bochiwal, H. Gorasia, S.D. Telang, C.N. Ramchand, Anal. Biochem. 356 (2006) 306–308.
[5] F.Q. Hu, L. Wei, Z. Zhou, Y.L. Ran, Z. Li, M.Y. Gao, Adv. Mater. 18 (2006) 2553–2556.
[6] J. Xie, C.J. Xu, Z.C. Xu, Y.L. Hou, K.L. Young, S.X. Wang, N. Pourmond, S.H. Sun, Chem. Mater. 18 (2006) 5401–5403.
[7] S. Santra, R. Tapec, N. Theodoropoulou, J. Dobson, A. Hebard, W.H. Tan, Langmuir 17 (2001) 2900–2906.
[8] H.H. Yang, S.Q. Zhang, X.L. Chen, Z.X. Zhuang, J.G. Xu, X.R. Wang, Anal. Chem. 76 (2004) 1316–1321.
[9] N. Sadeghiani, L.S. Barbosa, L.P. Silva, R.B. Azevedo, P.C. Morais, Z.G.M. Lacava, J. Magn. Magn. Mater. 289 (2005) 466–468.
[10] S. Sun, S. Anders, H.G. Hamann, J.-U. Thiele, J.E.E. Baglin, T. Thomson, E.E. Fullerton, C.B. Murray, B.D. Terris, J. Am. Chem. Soc. 124 (2002) 2884–2885.
[11] A. Kondo, H. Fukuda, Colloids Surf. A 153 (1999) 435–438.
[12] A.B. Lowe, B.S. Sumerlin, M.S. Donovan, C.L. Mccormick, J. Am. Chem. Soc. 124 (2002) 11562–11563.
[13] K. Ohno, K.-M. Koh, Y. Tsujii, T. Fukuda, Macromolecules 35 (2002) 8989–8993.
[14] Y. Zhang, N. Kohler, M. Zhang, Biomaterials 23 (2002) 1553–1561.
[15] I. Koh, X. Wang, B. Varughese, L. Isaacs, S.H. Ehrman, D.S. English, J. Phys. Chem. B 110 (2006) 1553–1558.
[16] E. Marutani, S. Yamamoto, T. Ninjbadgar, Y. Tsujii, T. Fukuda, M. Takano, Polymer 45 (2004) 2231–2235.
[17] M. Kamigaito, T. Ando, M. Sawamoto, Chem. Rev. 101 (2001) 3689–3746.
[18] B. Hu, A. Fuchs, S. Huseyin, F. Gordanine, C. Evrensel, Polymer 47 (2006) 7653–7663.
[19] N. Ayres, S.G. Boyes, W.J. Brittain, Langmuir 23 (2007) 182–189.
[20] K. Matyjaszewski, J. Xia, Chem. Rev. 101 (2001) 2921–2990.
[21] U. Jeong, X. Teng, Y. Wang, H. Yang, Y. Xia, Adv. Mater. 19 (2007) 33–60.

[22] N. Kohler, G.E. Fryxell, M. Zhang, J. Am. Chem. Soc. 126 (2004) 7206–7211.
[23] B. Gu, J.M. Armenta, M.L. Lee, J. Chromatogr. A 1079 (2005) 382–391.
[24] P. Wang, K.L. Tan, E.T. Kang, K.G. Neoh, J. Mater. Chem. 11 (2001) 783–789.
[25] C.A. Haynes, W. Norde, Colloid Surf. B 2 (1994) 517–566.
[26] R. Maoz, E. Frydman, S.R. Cohen, J. Sagiv, Adv. Mater. 12 (2000) 424–429.
[27] F. Stephen, R. Hakan, R.S. Nagaraja, F. Donald, Chem. Mater. 14 (2002) 3643–3650.
[28] S.H. Sun, H. Zeng, D.B. Robinson, S. Raoux, P.M. Rice, S.X. Wang, G.X. Li, J. Am. Chem. Soc. 126 (2004) 273–279.
[29] M. Yamaura, R.L. Camilo, L.C. Sampaio, M.A. Macedo, M. Nakamura, H.E. Toma, J. Magn. Magn. Mater. 279 (2004) 210–217.